Propulsion Characteristics Affecting the Aerodynamic Performance of an Externally Blown Flap Transport Model

Danny R. Hoad*
Langley Directorate, U.S. Army Air Mobility R&D Laboratory, Hampton, Va.

Two wind-tunnel investigations were conducted at Langley Research Center to determine the effect of different wake characteristics on the performance of two separate externally blown flap transport configurations. In both cases, the thrust removed lift coefficient could be directly related to the proportion of momentum captured by the flap system. In another investigation of an externally blown flap transport configuration, tufts were used to measure the upwash angles ahead of the wing. Using the thrust-removed lift coefficient, a simple vortex-lattice method provided a good approximation of these angles away from the nacelle inlets.

Nomenclature

A_f = total area of jet wake which impinges flap m^2
A_{if} = incremental area of jet wake which impinges flap m^2
A_j = total area of jet wake at flap m^2
c = local wing chord m
C_L = lift coefficient, lift/qs
$C_{L,TR}$ = thrust removed lift coefficient
C_μ = thrust coefficient, thrust/qs
P_A = engine-exhaust-flap impingement parameter
q = free-stream dynamic pressure N/m^2
q_{if} = incremental portion of jet which impinges flap, N/m^2
q_j = jet dynamic pressure at flap location, N/m^2
R = upper-half radius of nacelle, m
s = wing area, m^2
T = static thrust, N
z = vertical distance, m
α = angle of attack, degrees
δ = nominal flap deflection angle, degrees
δ_j = jet exhaust deflection (measured from body axis), $\tan^{-1}$ (normal force/axial force), degrees
θ = inflow angle, with respect to model horizontal axis, degrees
η = static thrust recovery efficiency, $[(\text{normal force})^2 + (\text{axial force})^2]^{1/2}/T$
ϕ = upflow angle, with respect to freestream degrees
BPR = bypass ratio
EBF = externally blown flap

Introduction

NUMEROUS high-lift concepts have been developed for achieving short-take-off-and-landing performance aircraft. One approach which was selected for an AMST configuration is the externally blown flap (EBF) YC15. Most EBF concept development has been concerned with experimental investigations[1-8] of various engine and airframe configurations. While very limited analysis[9-11] of these configurations has been attempted, some work has been done on an empirical analysis using a correlation parameter (impingement parameter) based on the vertical distance which the flap trailing edge extends into the jet exhaust from the engine center line, and the radius of the jet exhaust at the flap trailing edge.[12]

The present paper describes the results of a relatively simple analysis based on an engine exhaust flap area impingement parameter, which is a function of the distribution of dynamic pressure impingement on the flap, the area of the flap impingement, the total area of the engine exhaust, and the thrust. Isolated engine wake surveys were conducted to define this parameter for one of the EBF models for which aerodynamic performance data were available.[2] A uniform dynamic pressure profile was assumed to determine this parameter for the other EBF model correlation with aerodynamic performance data.[13]

A high-lift system, such as an EBF, induces large upflow angles in front of the wing in the region of the nacelle inlets. These flowfields must be defined in order that the nacelles be properly designed to minimize flow distortion at the engine face. This paper also presents the results of an investigation to measure the flow angle near the engine inlets of a representative EBF model. The vortex-lattice method[14] was used to calculate these upflow angles, to determine if they could be predicted.

Models

Exhaust Investigations

Two wind-tunnel investigations were conducted to determine the effect of different wake characteristics on the performance of two separate EBF transport configurations (Figs. 1 and 2).

A four-engine EBF transport (Model 1, Fig. 1) was tested in the Langley V/STOL tunnel. It had a 25° quarter-chord sweep, leading-edge slats deflected to 50°, and triple-slotted full-span flaps deflected to 0°, 20°, and 40°, respectively, for take-off configuration, and 15°, 35°, and 55°, respectively, for landing configuration. The engines were simulated by a two-part ejector similar to that in Fig. 3. Each engine simulator was fitted with five separate cowl assemblies intended to represent five different engine configurations (Fig. 4), which were designed to represent 1) TF-34, engine (BPR 6.2), 2) TF-34 with noise suppressor nozzle (Daisy nozzle), 3) stretched version of the TF-34 (Modified BPR 6.2), 4) JT-15D engine (BPR 3.2), and 5) high-bypass-ratio engine (BPR 10). The Modified BPR 6.2 was built such that the engine exit would be at the same chordwise location as the fan exit on the Daisy Nozzle. The BPR of these engine simulators does not describe in any way the size, horizontal position, or vertical position of the simulator, but is only intended to be a means of nomenclature. The important aspects of the simulator are not the characteristics at the exit, but the wake characteristics at the location of the flap, as will be evident later in this paper. For further details of this model see Ref. 2.

A two-engine straight wing EBF transport (model 2, Fig. 2) was tested in the 5.18-m test section of the Langley 300-mph

Presented as Paper 75-1218 at the AIAA/SAE 11th Propulsion Conference, Anaheim, Calif., Sept. 29-Oct. 1, 1975; submitted Sept. 24, 1975; revision received Nov. 25, 1975.

Index categories: Aircraft Aerodynamics (including Component Aerodynamics); Aircraft Performance.

*Aerospace Engineer, Low-Speed Aerodynamics Branch, Subsonic-Transonic Aerodynamics Division. Member AIAA.

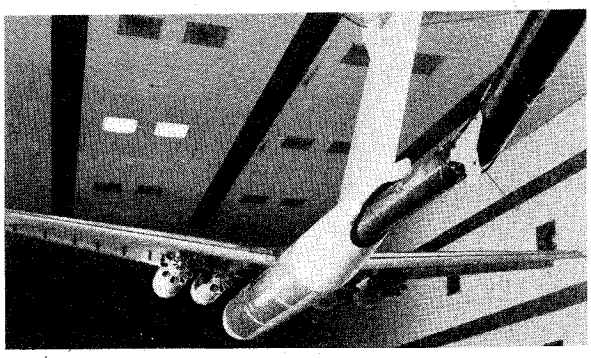

Fig. 1 Model 1 in Langley V/STOL tunnel (Daisy nozzle engines).

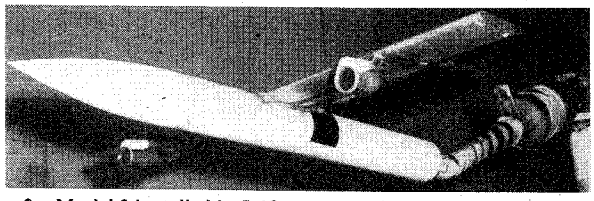

Fig. 2 Model 2 installed in 5.18-m test section of Langley 300-mph 7- by 10-ft tunnel.

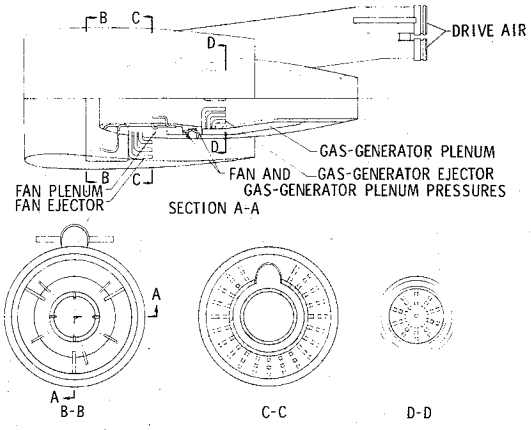

Fig. 3 Two-part engine simulator, Model 1.

7- by 10-ft tunnel. It had a leading-edge slat deflected to 40°, a double-slotted flap deflected to 40° for the take-off configuration, and a triple-slotted flap deflected to 60° for the landing configuration. The engines were simulated by a two-part ejector as presented in Fig. 5. The engine vertical position on this configuration was varied (to three positions) to determine its effect on the performance of the configuration (Fig. 6).

Inlet Investigation

The model presented in Fig. 1 was also used as a source of propulsive lift to determine the upflow angles ahead of the wing. A tuft grid used to indicate these flow angles was attached to the outboard side of the port nacelle. Wire standoff masts were used to decrease the interference of the supporting frame and to set the tufts at the desired vertical and longitudinal location at a spanwise station midway between the port nacelles. Four long tufts were installed on staffs long enough to place the tufts on the vertical plane of the outboard port nacelle inlet (Fig. 7).

Test

Both models were mounted on a sting-supported six-component strain-gage balance for measurements of the total forces and moments.

Isolated engine-exhaust-wake surveys were conducted for each engine configuration on Model 1 so that the exhaust-flap

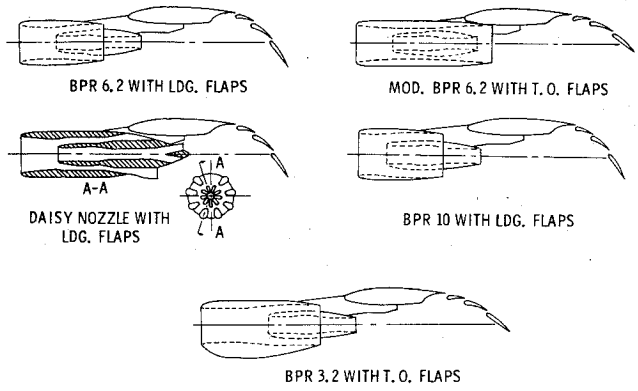

Fig. 4 Engine configurations used on Model 1.

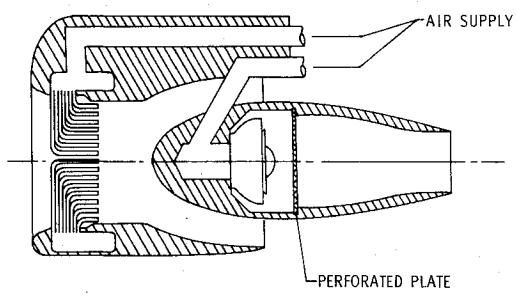

Fig. 5 Two-part ejector, Model 2.

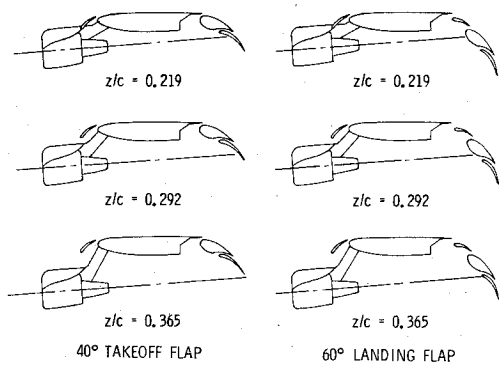

Fig. 6 Engine positions used on Model 2.

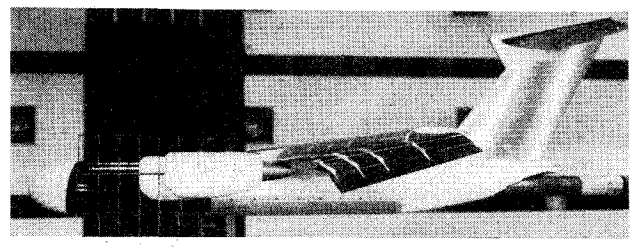

Fig. 7 Tuft grid mounted between nacelles of STOL Model 1. 50° slats and landing flaps.

area impingement parameter could be determined. Dynamic-pressure measurements were made with a pressure rake positioned so that the probes were alined along a radial line from the geometric center line. Four radial positions were chosen for the Daisy Nozzle and two radial positions were chosen for the other four engine simulators. These profiles were repeated at various downstream locations to obtain dynamic-pressure profile characteristics. Isolated engine wake surveys were not available for the engine simulators on Model 2. Since the same engine was used in all three positions, it was felt that assuming a 10° spread angle would be sufficient to

determine the relative influence of the exhaust-flap area impingement parameter.

Jet-deflection angles δ_j and static-thrust recovery efficiency η for both models were determined from measurements of the normal and axial forces made in the static thrust condition with flaps deflected and leading-edge slat deployed.

Calculations

Exhaust Characteristics

Isolated engine wake surveys were available for each engine configuration used on Model 1. The flap impingement parameter was computed using the distribution of dynamic pressure at the flap location in the following manner

$$P_A = \left\{\sum q_{if} A_{if}\right\} \frac{S}{TA_j} \sin \delta_f$$

The wing area is provided only as an arbitrary constant to nondimensionalize P_A.

Since isolated engine surveys were not available for the engine configuration used on Model 2, the dynamic pressure was assumed uniform at the flap location. The exhaust was assumed to spread at an angle of 10° to determine the size of the exhaust at the flap location. The impingement parameter in this case is slightly simplified in that the dynamic pressure is assumed constant over the flap.

$$P_A = \frac{q_j A_f S}{T A_j} \sin \delta_f$$

The lift developed by a powered-lift system can be separated into three parts according to the source of the lift, 1) the lift that would have been produced by the unpowered wing, 2) the lift due to the component of the jet which has been redirected by the flap system, and 3) the lift due to circulation induced by the blowing. If the portion of the lift due to the component of the jet, which has been directed by the flap system, is removed from the total lift in the following manner

$$C_{L,TR} = C_L - \eta\, C_\mu \sin(\delta_j + \alpha)$$

a thrust-removed lift coefficient remains which can be related to the flap impingement parameter. This thrust-removed lift coefficient is also useful in the analysis of the upwash angles ahead of the wing.

Inlet Characteristics

As a comparison to the experimentally determined upwash angles measured on Model 1, these angles were estimated using the vortex lattice method. The thrust-removed lift coefficient and wing geometric characteristics were used in a vortex lattice program[14] to determine the magnitude and distribution of local section lift coefficient, from which the distribution of circulation was determined. Using the distribution of circulation, flowfield velocity components were determined which, in turn, defined the flow angle. The program did not account for thickness effects, nacelle inlets, or the inflow into the nacelle inlets. The local angle of attack and circulation were extracted from the program of Ref. 14 and input into a flowfield program, derived from the vortex lattice method, to compute the upflow angle ϕ ahead of the wing. The experimental angle of attack was then added to the upflow angle to obtain the total inflow angle θ.

Results and Discussion

The flap static turning effectiveness parameters are presented in Fig. 8 for both models in polar coordinate form. These parameters for the five engine simulators on Model 1 and the three positions of the engine simulator on Model 2 in the take-off and landing configurations are presented at a thrust which

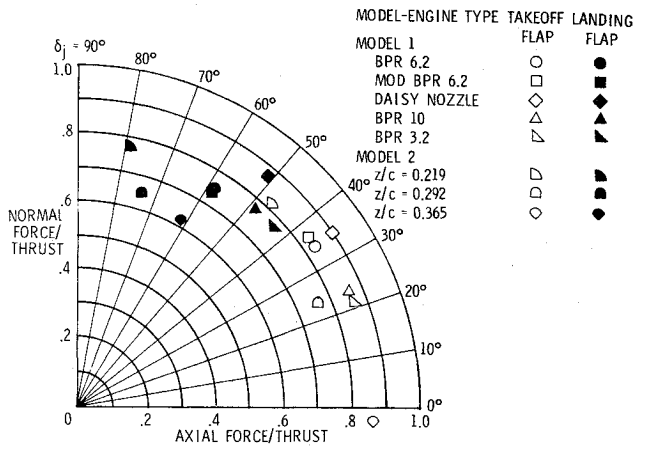

Fig. 8 Flap static turning effectiveness parameters (Models 1 and 2).

would correspond to a thrust coefficient of 2 with the forward speed tested in each configuration.

A perpendicular distance from a data point in Fig. 8 to the horizontal axis would represent the lift component due to thrust at an angle of attack of 0°. If it were assumed that with zero power all engine simulator configurations had identical characteristics and that the only additions to the aerodynamic characteristics at an angle of attack of 0° are those components in Fig. 8, an assessment could be made as to the relative merit of the configurations. As discussed in Ref. 2, this assessment of the aerodynamic characteristics of an engine-model configuration is not necessarily true. A more pertinent comparison based on the engine-exhaust impingement area parameter is presented later in this paper.

The exhaust-flap area impingement parameter is a correlation parameter which relates the engine-exhaust properties with the performance of the engine-model configuration. The lift coefficient performance and impingement parameter is presented in Table 1 for several model flap combinations at zero angle of attack.

The effect of engine configuration (Fig. 9) for the landing flap indicates that the engine-model combination which produces the largest impingement parameter, BPR 6.2 and Modified BPR 6.2, provides the largest lift coefficient. The combination which produces the smallest impingement parameter (BPR 3.2) provides the smallest lift coefficient. This impingement parameter is really a measure of the proportion of $q_j A_j$ or momentum which impinges on the flap, which in turn is deflected and induces circulation. This would indicate that the more momentum captured by the flap system, the better the combination will perform. The effect of engine configuration for the take-off flap (Fig. 10) is similar except for the relative performance and magnitude of impingement parameter for the Daisy Nozzle. The Daisy Nozzle has eight fan lobes and nine gas generator lobes. Since the wake survey for this engine included only two fan lobes and two gas generator lobes, it was not comprehensive enough to adequately define the profile.

The comparisons of the performance and impingement parameter for Model 2 with landing flap and take-off flap are presented in Figs. 11 and 12. The results of the landing flap configuration indicate that moving the engine exhaust ver-

Table 1 Lift coefficient performance and impingement parameter

Figure	Model	Flap
9	1	Landing
10	1	Take-off
11	2	Landing
12	2	Take-off

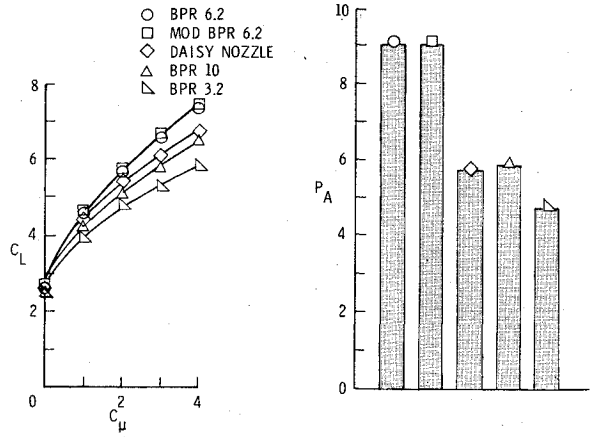

Fig. 9 Performance and impingement parameter comparison (Model 1 with landing flaps, $\alpha = 0°$).

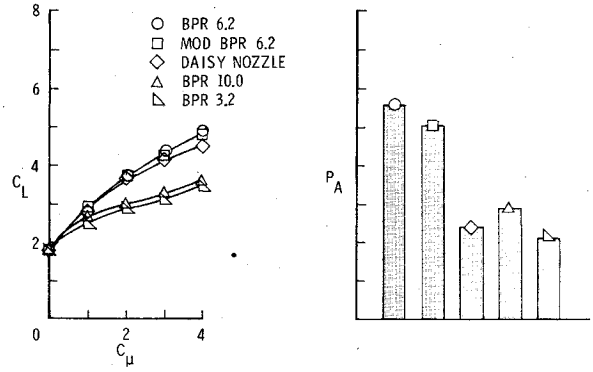

Fig. 10 Performance and impingement parameter comparison (Model 1 with take-off flaps, $\alpha = 0°$).

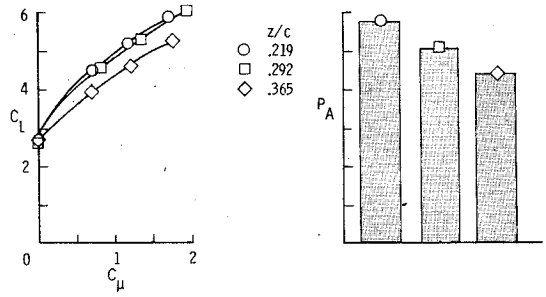

Fig. 11 Performance and impingement parameter comparison (Model 2 with landing flaps, $\alpha = 0°$).

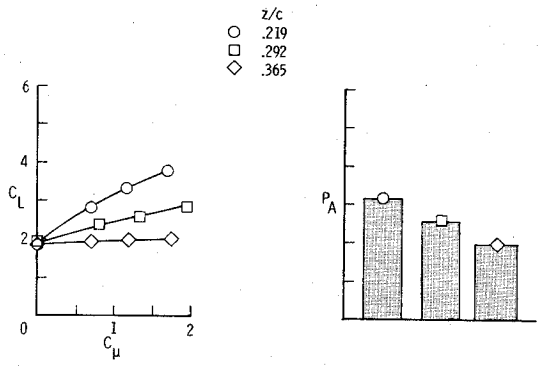

Fig. 12 Performance and impingement parameter comparison (Model 2 with take-off flaps, $\alpha = 0°$).

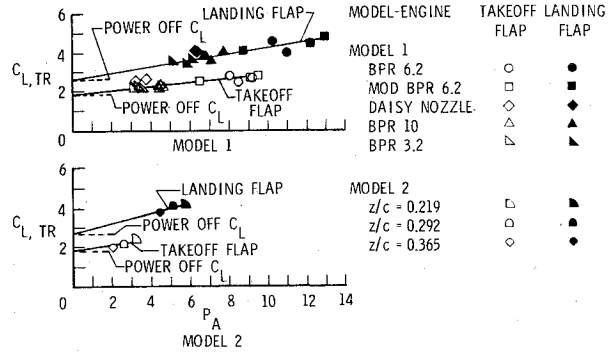

Fig. 13 Impingement parameter and thrust-removed lift coefficient comparison. $\alpha = 0°$

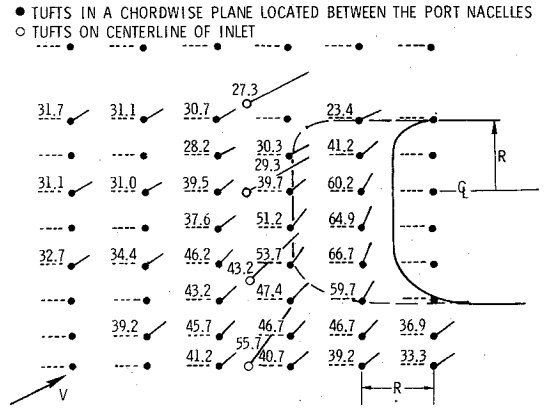

Fig. 14 Tuft pattern ahead of wing of Model 1. (Landing flap, $C_\mu = 2.0$, $\alpha = 25.7$, $C_L = 6.75$.)

tically toward the wing lower surface increases the proportion of $q_j A_j$ or momentum which is captured by the flap system, and in turn generates increased lift. Figure 12, take-off flap, indicates the same trend, however, at a somewhat lower value, which can be attributed to less flap projection to capture the exhaust.

To further tie this engine-flap area impingement parameter with the lift performance of the models, the thrust-removed lift coefficient at zero angle of attack was computed for each condition and presented in Fig. 13 as a function of the impingement parameter. The data for both models at each flap deflection are presented in this figure. It is evident that the thrust-removed lift coefficient is the prime aerodynamic factor which can be related to the impingement parameter, evidenced by the data fitting a straight line which intercepts $P_A = 0$ at the value of C_L which corresponds to the power-off condition (P_A should be zero in this case). If the blowing did not induce supercirculation lift these data points would be on horizontal lines. In each model it can be seen that the landing configuration data describe a line with a larger slope than that of the take-off configuration. This is more evidence that since the landing flaps capture more of the exhaust flow, more circulation lift is induced. This again emphasizes the fact that the engine-exhaust flap area inpingement parameter is a measure of the proportion of momentum captured by the flap, and in turn provides a method to assess the relative performance of engine-wing configurations.

Inlet Investigation Results

A sketch of the tuft pattern of flow angles in the body axis at a given condition is presented in Fig. 14 for Model 1 with a landing flap, thrust coefficient of 2, 25.7°angle of attack, and lift coefficient of 6.75. These results show that the inflow angle θ can be as high as 67°between and near the nacelles. The tufts mounted on the engine vertical plane of symmetry indicate the angle of flow induced by the engine inlet, which is somewhat less than the adjacent flow between the nacelles.

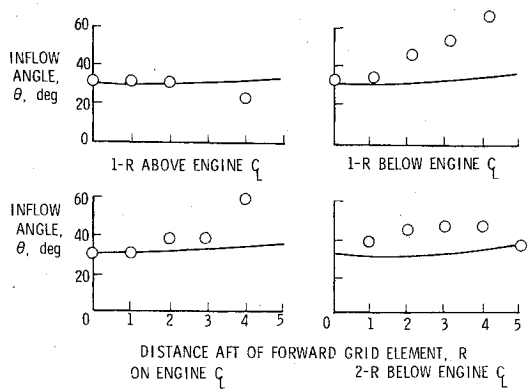

Fig. 15 Experimental and calculated inflow angles ahead of wing (Model 1).

Figure 15 presents a comparison of the experimental results with the calculated angles based on the thrust-removed lift coefficient. The inflow angles are presented for the following tuft rows where the vertical distance from the engine center line is nondimensionalized by nacelle radius: $z/r = 1, 0, -1, -2$. The horizontal scale presents the tuft locations as a function of nacelle radii from front to rear.

The method of calculation appears to be useful, showing fair agreement in the region away from the nacelle inlet. The calculations near the nacelle inlet are lower than the experimentally measured angles. The program does not represent the geometry of the large nacelles or the inlet flow induced by them, therefore, the flows around and between these nacelles are not well estimated.

Concluding Remarks

This paper provides a technique to assess the relative lift performance of EBF configurations based on an exhaust-flap impingement parameter which is a function of the proportion of momentum which is captured by the flap system. It was shown that the lift produced by an EBF configuration can be related to the proportion of momentum captured by the flap system and that the thrust-removed lift coefficient can be directly related to this captured momentum, defined by the engine exhaust-flap area impingement parameter.

This paper also presents the results of a wind-tunnel investigation designed to measure the upwash ahead of the wing of a representative EBF configuration. It was shown that the upwash ahead of the wing of a high-lift system can be estimated by a simple vortex lattice method using the thrust-removed lift coefficient to generate the distribution of local section lift coefficient, which in turn is used to generate the distribution of circulation. This was then used to compute flowfield velocities, which define the flow angles.

References

[1] "STOL Technology," Ames Research Center, Moffett Field, Calif., ASA, SP-320, Oct. 1972.

[2] Hoad, D.R., "Longitudinal Aerodynamic Characteristics of an Externally Blown Flap Powered-Lift Model with Several Propulsive System Simulators," Langley Directorate, USAAMRDL, Hampton, Va., NASA, TN D-7670, Sept. 1974.

[3] Parlett, L.P., Freeman, D.C., Jr. and Smith, C.C., Jr., "Wind-Tunnel Investigation of a Jet Transport Airplane Configuration With High Thrust-Weight Ration and an External-Flow Jet Flap," NASA TN D-6058, 1970.

[4] Smith, C.C. Jr., "Effect of Wing Aspect Ration and Flap Span on Aerodynamic Characteristics of an Externally Blown Jet-Flap STOL Model," NASA TN D-7205, 1973.

[5] Parlett, L.P., Smith, C.C., Jr., and Megrail, J.L., "Wind-Tunnel Investigation of Effects of Variations in Reynolds Number and Leading-Edge Treatment on the Aerodynamic Characteristics of an Externally Blown Jet-Flap Configuration," NASA TN D-7194, 1973.

[6] Aoyagi, K., Falarski, M.D., and Koenig, D.G., "Wind-Tunnel Investigation of a Large-Scale 25°Swept-Wing Jet Transport Model With an External Blowing Triple-Slotted Flap," NASA TM X-62197, 1973.

[7] Freeman, D.C., Jr., Parlett, L.P., and Henderson, R.L., "Wind-Tunnel Investigation of a Jet Transport Airplane Configuration With an External-Flow Jet Flap and Inboard Pod-Mounted Engines," NASA TN D-7004, 1970.

[8] Vogler, R.D., "Wind-Tunnel Investigation of a Four-Engine Externally Blowing Jet-Flap STOL Airplane Model," NASA TN D-7034, 1970

[9] Johnson, W.G., Jr. and Kardas, G.E., "A Wind-Tunnel Investigation of the Wake Near the Trailing Edge of a Deflected Externally Blown Flap," NASA TM X-3079, 1974.

[10] Goldhammer, M.I., Lopex, M.L., and Shen, C.C., "Methods for Predicting the Aerodynamic and Stability and Control Characteristics of STOL Aircraft – Volume 1, Basic Theretical Methods," Douglas Aircraft Company, McDonnell Douglas Corporation, Tech. Rept. AFFDL-TR-73-146, Dec. 1973.

[11] May, F. and Widdison, C.A., "STOL High-Lift Design Study – Volume 1, State-of-the-Art Review of STOL Aerodynamic Technology," The Boeing Company, Tech. Rept. AFFDL-TR-71-26, April 1971.

[12] Roe, M.H., Renselaer, D.J., Quam, R.A., et al., "STOL Tactical Aircraft Investigation – Externally Blown Flap – Volume 2, Design Compendium," Los Angeles Aircraft Division, Rockewll International Corporation, AFFDL-TR-73-20, April 1973.

[13] Johnson, W.G., Jr., "Longitudinal Aerodynamic Characteristics of a Wing-Body Combination Having a Rectangular, Aspect-Ratio-6, Slotted Supercritical Wing With Externally Blown Flaps," NASA TM X-2388, 1971.

[14] Margason, R.J. and Lamar, J.E., "Vortex-Lattice Fortran Program for Estimating Subsonic Aerodynamic Characteristics of Complex Planforms," NASA TN D-6142, 1971.